M.S. Veshchunov

MODELLING OF ZIRCALOY CLADDING HYDRIDING IN HIGH BURNUP FUEL TESTS

УДК 621.329

Вещунов М.С. МОДЕЛИРОВАНИЕ ПРОЦЕССОВ ГИДРИРОВАНИЯ ZRY ОБОЛОЧЕК ТВЭЛОВ В ЭКСПЕРИМЕНТАХ С ГЛУБОКИМ ВЫГОРАНИЕМ ТОПЛИВА. Препринт № IBRAE-99-08. Москва: Институт проблем безопасного развития атомной энергетики РАН. 1999. 14 с. Библиогр.: 19 назв.

Аннотация

В настоящей работе предпринята попытка моделирования поглощения водорода Zry оболочками твэлов PWR в процессе окисления в экспериментах с глубоким выгоранием топлива. Развиваемая модель основана на ранее предложенном механизме проникновения водорода в металлическую часть оболочки через растущий слой оксида, в совокупности с моделированием многокомпонентной диффузии кислорода и водорода через двухфазную область в металлической зоне оболочки (включающую растущие гидриды). В результате такого подхода удается естественным образом объяснить наблюдаемое сильно неоднородное распределение гидридов по металлической зоне, которое, в соответствие с современными представлениями, приводит к механическому охрупчиванию оболочек и разрушению твэлов в экспериментах с глубоковыгоревшим топливом.

Veshchunov M.S. MODELLING OF ZIRCALOY CLADDING HYDRIDING IN HIGH BURNUP FUEL TESTS. Preprint IBRAE-99-08. Moscow: Nuclear Safety Institute. November 1999. 14 p. — Refs.: 19 items.

Abstract

Modelling of the complicated behaviour of hydrogen in the oxidising Zry cladding observed in the high burnup fuel tests, is attempted. The developed model is based on the previous approach to the description of the hydrogen penetration mechanism through the growing oxide scale of the Zr cladding, self-consistently combined with modelling of the multicomponent (hydrogen-oxygen) diffusion in the two-phase zone (hydrides in the metal matrix). As a result, this allows natural explanation of the observed steep spatial gradients in the hydride distribution over the Zr cladding, leading to the brittle mechanical behaviour of the cladding and PCMI failure of the high burnup fuel rods.

Modelling of Zircaloy Cladding Hydriding in High Burnup Fuel Tests

M.S. Veshchunov

Nuclear Safety Institute (IBRAE), Russian Academy of Sciences

B.Tul'skaya, 52, Moscow, 113191

phone: (095) 955 2618, fax: (095) 958 0040, e-mail: vms@ibrae.ac.ru

I.   Introduction

1. Recent results from reactivity initiated accident (RIA) experiments with high burnup fuel [1,2] indicate that the safety criteria which have been formulated on basis of fresh or low burnup fuel experiments may not be applicable to high burnup fuel rods. In these experiments fuel rod failures occurred well below the regulatory level and with clear indications for a pellet-cladding material interaction (PCMI) failure mode, characteristic for high burnup fuel and not observed in the earlier fresh and low burnup fuel tests. Currently the internationally agreed failure mode is the hydride assisted PCMI failure [3].

High burnup fuel cladding of the Pressurised Water Reactors (PWR) is characterised by severe and typical corrosion phenomena. Waterside corrosion produces the deposition of a steadily increasing oxide layer on the cladding surface and simultaneous hydrogen absorption in the metallic part with a steep radial gradient of hydride spatial distribution over the clad thickness. These corrosion effects lead to a brittle mechanical behaviour of the cladding material and in particular, to the shift of the brittle to ductile transition to high temperatures [1,2].

In the tests without spalling of the oxide layer the clad failure was attributed to a steep hydrogen gradient in the clad wall. Such a distribution of hydrides was observed in the French experiments CABRI of the REP-Na series [1,3] (Fig. 1), as well as in the Japanese experiments NSSR of the HBO series [2] (Fig. 2). The generation of parallel cracks in the heavily hydrided zone where one of the cracks penetrates cladding wall and the other stopped in the middle of wall thickness, can be clearly seen in Fig. 2.

2. A non-homogeneous hydride spatial distribution in the metal cladding observed in the above mentioned experiments seems at the first glance to be rather unexpected and demands a detail explanation, owing to the important consequences of such a behaviour (i.e. clad failure). Indeed, one should apparently expect rather quick (in comparison with a slow growth of the oxide scale) hydrogen spatial homogenisation in the metal zone, owing to the extremely high diffusivity of hydrogen atoms dissolved in the Zry. Namely such a homogeneous distribution of hydride platelets in the metal cladding (under uniform hydride layer near the surface) is usually observed in the tests on Zry gaseous hydriding (without protective oxide scale) in the pure hydrogen atmosphere after several hours (see, for example, [4-6]).

However, there is no complete analogy between the two mentioned types of experiments. As emphasised in [4], in surveying the results on hydrogen absorption one should clearly distinguish between two possible routes; first, direct reaction with molecular hydrogen (gaseous hydriding), and second, absorption of hydrogen liberated by the decomposition of water or steam during the oxidation process and absorbed as part of the oxidation mechanism.

The most important differences between these two phenomena are amounts and rates of hydrogen absorbed in the metal phase, since an oxide scale on the metal surface strongly protects Zry from direct hydrogen penetration. As a result, at the same temperatures (350-450°C) the amount of dissolved atomic hydrogen in the cladding wall attains its solubility limit in a few hours in the first case (gaseous hydriding) [6], whereas several reactor irradiation cycles are necessary for noticeable hydride precipitation in the high burnup fuel cladding [3], corresponding to the second case (hydrogen absorption during oxidation process).

Another peculiarity of the hydrogen absorption phenomenon in the oxidising cladding is that rapid redistribution of atomic hydrogen (penetrated through the oxide scale) and hydride formation inside the metal wall occur simultaneously with a relatively slow oxygen diffusion front penetration in the same metal zone.

Resulting oxygen concentration gradient furnishes spatially inhomogeneous conditions for the hydride precipitation and growth in the metal matrix.

The first phenomenon of hydrogen penetration through the oxide scale during oxidation process was thoroughly studied experimentally either at low temperatures 350 - 500°C (see, for example, review [4]), or at high temperatures 900 - 1200°C (mainly in recent experiments [7]). For the description of the high temperature experiments [7] a kinetic model was developed by the author and Berdyshev [8] which considers a new mechanism for hydrogen penetration through the oxide scale and satisfactorily simulates available experimental data on the kinetics of hydrogen absorption by oxidising Zr-1Nb alloy. Lacking exhaustive kinetic data at lower temperatures, the model was not attempted to be applied to the low temperature case, however, as indicated in [8], in general it qualitatively corresponds to the observations of significant hydrogen uptake (up to tens percents of a total amount of generated hydrogen) during Zr oxidation in a broader temperature range.

Another problem concerning self-consistent description of hydrogen and oxygen diffusion transport in the metal Zr cladding accompanied by precipitation and growth of hydrides in the bulk of the metal matrix, was not studied theoretically, since in the high temperature (900-1200°C) oxidation tests hydrogen was dissolved in the metal phase in the atomic form, without hydride precipitation. However, a similar physical problem of multicomponent diffusion in a two-phase zone was earlier investigated in the papers of the author and Hofmann, in which a new approach to the general theoretical problem was developed and applied to the kinetic description of B_4C interactions with Zry [9] and stainless steel (s.s.) [10]. In both studied cases the two-phase region consisting of precipitates of one phase in the bulk of another phase appeared in the reaction zone. Moreover, in the case of B_4C/s.s. interactions boride precipitates were distributed in the s.s. matrix rather inhomogeneously, similarly to hydride distribution in the Zry cladding in the high burnup fuel tests [1,2].

II.   Physical mechanisms of hydrogen absorption

In the present paper explanation and theoretical description on the qualitative level (in the lack of detailed experimental data) of the complicated behaviour of hydrogen in the oxidising Zr cladding observed in the high burnup fuel tests, are attempted. The developed model is based on the previous approach to the description of the hydrogen penetration mechanism through the growing oxide scale of the Zr cladding, self-consistently combined with modelling of the multicomponent (hydrogen-oxygen) diffusion in the two-phase zone (hydrides in the metal matrix). As a result, it allows natural explanation of the observed steep spatial gradients in the hydride distribution over the Zr cladding, leading to the brittle mechanical behaviour of the cladding and PCMI failure of the high burnup fuel rods. In the present section a brief description of the previously developed mechanisms of: (i) hydrogen absorption by Zr alloys during oxidation in steam and mass transfer through the growing oxide scale at high temperatures (which will be further applied to the low temperature case); and (ii) diffusion mass transfer in the two-phase region (which will be further applied to the heavily hydrided metal zone of oxidising Zr cladding), is presented.

II.1.   Mass transfer mechanism through the oxide scale

The model of hydrogen absorption by Zr alloys during high-temperature (900 - 1200°C) oxidation in steam [8] is essentially based on the detailed experimental results of the recent tests [7]. The main obstacle for an appropriate interpretation of this important phenomenon in the literature was connected with numerous results on gaseous hydriding of zirconia which directly evidenced that hydrogen solubility and mobility in oxide layers are negligibly small. On this basis it was generally believed that a very thin oxide layer (with a thickness of several μm) on the metal surface protects the metal substrate from hydrogen penetration, and the observed high values of hydrogen absorption during oxidation in steam were mainly associated with defect structure (e.g. cracks or pores) of the growing protective oxide layer.

However, as mentioned above, one should distinguish between direct gaseous hydriding of non-oxidised metal cladding and hydrogen absorption as part of the oxidation mechanism [4]. This conclusion can be indirectly confirmed by the results of Wagner's tests [11] on water vapour absorption by yttria-stabilised zirconia in which interaction process was interpreted in terms of the reaction: $H_2O(g) + V_O^{2+} = 2H_i^+ + O_O(ox)$, with positively charged protons H^+ in the solid solute rather than neutral atoms characteristic for gaseous hydriding experiments (e.g. [12]). It was proposed in [12] that this fundamental difference in the two dissolution

processes can explain an essential increase of positively charged proton solubility and mobility (detected in [11]) in comparison with neutral H atoms.

In the paper [8] on the basis of this important qualitative conclusion, the standard consideration of the steam oxidation process in the framework of the coupled anodic/cathodic reactions at the two oxide interfaces (gas/oxide and oxide/metal) was modified, taking into account that hydrogen may intrude into oxide in the result of the H_2O dissolution process governed by the same mechanism as observed in the tests [11], i.e. in the form of positively charged protons. Discharge of protons by electrons in this scheme occurs mainly at the oxide/metal interface (rather than at the gas/oxide interface as considered in the standard approach) after diffusion transporting of highly mobile protons through the oxide scale. For a quantitative description of the hydrogen behaviour by this mechanism, mass transfer in the three layers: gas, oxide and metal, and at corresponding interfaces: gas/oxide and oxide/metal, was considered.

Modelling of mass transfer through the oxide/gas interface was based on the consideration of equilibrium kinetic processes in the vicinity of the oxide surface:

- dissolution of water molecules at the oxide surface:

$$H_2O(g) + V_O^{2+} = 2H_{ab}^+ + O_O(ox);$$
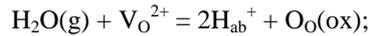
- dissociation of water molecules in the gas phase:

$$2H_2O(g) = O_2(g) + 2H_2(g);$$
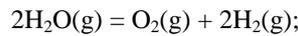
- transitions from the oxide to the gas phase of oxygen:

$$2O_O(ox) = O_2(g) + 2V_O^{2+} + 4e_\beta(ox/g);$$

and hydrogen:

$$H_{ab}^+(ox) + e_\beta(ox/g) = H_{ab}(ox) = (1/2)H_2(g),$$
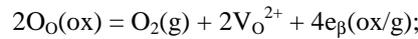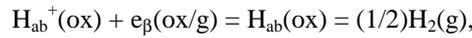
which are described by the corresponding mass action laws. In particular, such a consideration allows specification of the thermodynamic boundary conditions for the proton $H_{ab}^+(ox)$ concentration C_{H+} and the hydrogen gas surface pressure $p_{H2}(s)$ at the gas/oxide interface under steam normal oxidation conditions:

$$C_{H+} \propto (p_{H2}(s)/RT)^{1/4}, \tag{1}$$

and explains high concentration of dissolved protons in comparison with concentration C_H of neutral hydrogen atoms $H_{ab}(ox)$ dissolved in the oxide. Indeed, in accordance with equilibrium reaction at the interface:

$$H_{ab}(ox) = (1/2)H_2(g),$$
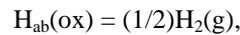
C_H obeys usual Sieverts' law:

$$C_H \propto (p_{H2}(s)/RT)^{1/2}, \tag{2}$$

and, hence, under condition $p_{H2}(s)/p_{H2O} \ll 1$, satisfies the above mentioned relationship, $C_H \ll C_{H+}$. Otherwise, under steam starvation conditions when $p_{H2O}/p_{H2} \to 0$, for the proton concentration in the oxide, instead of Eq. (1) one gets:

$$C_{H+} \propto p_{H2O}^{1/3} p_{H2}^{1/6}. \tag{3}$$

Therefore, in the tests on Zr gaseous hydriding (i.e. $p_{H2O} \to 0$) hydrogen is to be dissolved in the atomic neutral form obeying Sieverts' law, Eq. (2), in accordance with observations [12], since the proton concentration in this case turns to zero, $C_{H+} \to 0$.

Mass transfer in the oxide phase is treated by self-consistent considerations of diffusion transport of oxygen ions and protons:

$$J_O^{(ox)} = D_O^{(ox)} \Delta C_O / \delta(t), \tag{4a}$$

$$J_H^{(ox)} = D_H^{(ox)} \Delta C_{H+} / \delta(t), \tag{4b}$$

where $D_O^{(ox)}$ and $D_H^{(ox)}$ are the oxygen and hydrogen ions diffusivities in the oxide, respectively; ΔC_O and ΔC_{H+} are the oxygen and hydrogen concentration falls across the oxide layer, respectively; $\delta(t)$ is the oxide layer thickness determined by the self-consistent solution of the oxygen diffusion problem in the multilayered gas/oxide/metal system (in the high temperature tests being proportional to $t^{1/2}$).

The value of $D_H^{(ox)}$ measured in [11] has the same order of magnitude as $D_O^{(ox)}$. A possible explanation of a very high mobility of protons in comparison with neutral hydrogen atoms (measured in [12]) is that both protons and oxygen ions must penetrate the solid at the same rate to preserve local electrical neutrality in the crystal. Since diffusivity of negatively charged oxygen ions in zirconia is rather high, they carry along positively charged protons in the same direction.

The anodic reactions at the metal/oxide interface considered as equilibrium:

$$ZrO_2(ox) + 2V_O^{2+} + 4e_\alpha(m/ox) = Zr(m) + 2O_O(ox),$$

and

$$H_{ab}^+(ox) + e_\alpha(ox/m) = H_{ab}(m),$$
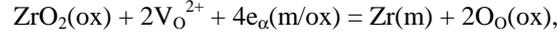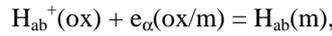
allow application of the mass action law for these reactions, resulting in a simple linear relationship between interface hydrogen concentrations in the oxide $C_{H+}(b)$ and in the metal $C_H^{(m)}|_I$:

$$C_{H+}(b) = \gamma C_H^{(m)}|_I ,$$

that provides boundary conditions for the diffusion problem either in the oxide phase or in the metal phase.

The obtained system of equations was qualitatively and quantitatively analysed in [8] explaining the main features of the observed complicated kinetics of hydrogen uptake at high temperatures: (i) continuous increase of hydrogen concentration in the metal phase being roughly proportional to the oxidation mass gain, in the initial stage of the process; (ii) desorption of hydrogen to the gas phase accompanied by slow decrease of measured hydrogen concentration in the metal phase, in the late stage of the process; (iii) decrease of maximum hydrogen concentration in Zr attained at the absorption/desorption regime transformation, with temperature increase. Numerical solution of the problem generally confirmed the main conclusions of the qualitative treatment and furnished a satisfactory fitting between measured in [7] kinetic curves and calculations.

II.2.   Mass transfer mechanism through the two-phase zone

The main difficulty in modelling of mass transfer in the metal zone of the cladding is connected with the appearance of the extended two-phase region of hydride precipitates in the Zr matrix. The formation of a two-phase zone as a result of chemical interactions in multicomponent systems is a rather common phenomenon studied by the author of the present paper and Hofmann in particular cases of B_4C/Zry [9] and B_4C/s.s. interactions [10]. A new approach for the solution of the general problem was formulated in [9,10]. Being applied to the specific ternary system B-C-Zr it allowed adequate description of the kinetics of the B_4C/Zry interactions. However, the distribution of the second phase precipitates along the two-phase zone of the B_4C/Zry interactions couple was quite homogeneous, and that allowed significant simplification of the model developed in [9]. In the situation of B_4C/s.s. interactions the distribution of boride precipitates in the s.s. matrix was essentially inhomogeneous, since the amount of these precipitates decreased continuously with increasing distance from the B_4C/s.s. interface.

As indicated in [9,10], the description of mass transfer through a two-phase zone in multicomponent systems is based on the generalisation of the Flemings approach [13,14] for modelling an analogous process in a binary system in an inhomogeneous temperature field. The main idea of the approach [14] was based on the assumption that the two phases were in local equilibrium with each other in the entire bulk of the two-phase layer. For the binary system this condition of local equilibrium can be fulfilled simultaneously with the condition of existence of concentration gradients inside both phases (providing diffusion mass transfer) only in the external inhomogeneous temperature field.

In a ternary system these both conditions can be fulfilled simultaneously in the absence of temperature gradients, this is based on general thermodynamic properties of the equilibrium ternary phase diagrams (see [9,10]). As an example, this can be demonstrated by a consideration of an isothermal section of the schematic low temperature Z-O-H phase diagram in Fig. 3. Similarly to the previously considered case of B_4C/s.s.

interactions [10], the part *DE* of the diffusion path crosses the two-phase area of the phase diagram, and each point of this line *DE* (e.g. point *F*) describes equilibrium states of the two phases with compositions corresponding to the ends of equilibrium tie-lines (*ff'*) crossing this point (*F*) (so-called „lever rule").

As the diffusion path propagates through the two-phase area in Fig. 3, compositions of the phases are changed continuously in accordance with this rule (points $d \rightarrow f \rightarrow e$ for one phase and $d' \rightarrow f' \rightarrow e'$ for the other), and, simultaneously, local equilibrium between the two phases (e.g. points $d \leftrightarrow d'$, $f \leftrightarrow f'$, $e \leftrightarrow e'$) is sustained in all spatial points of the reaction zone.

Quantitative description of mass transfer in such a ternary system is reduced to the system of two diffusion-type equations:

$$\partial/\partial t[c_1(x,t)(1-f(x,t)) + c_2(x,t)f(x,t)] = D_c^{(1)}\partial/\partial x[(1-f)\partial c_1/\partial x] + D_c^{(2)}\partial/\partial x(f\partial c_2/\partial x)$$

$$+ D_{cb}^{(1)}\partial/\partial x[(1-f)\partial b_1/\partial x] + D_{cb}^{(2)}\partial/\partial x(f\partial b_2/\partial x), \tag{5a}$$

$$\partial/\partial t[b_1(x,t)(1-f(x,t)) + b_2(x,t)f(x,t)] = D_b^{(1)}\partial/\partial x[(1-f)\partial b_1/\partial x] + D_b^{(2)}\partial/\partial x(f\partial b_2/\partial x)$$

$$+ D_{bc}^{(1)}\partial/\partial x[(1-f)\partial c_1/\partial x\} + D_{bc}^{(2)}\partial/\partial x(f\partial c_2/\partial x), \tag{5b}$$

where b_1, c_1 and b_2, c_2 are concentrations of the diffusing components (e.g. H and O) in the coexisting phases 1 (e.g. metal Zr) and 2 (e.g. δ-hydride ZrH$_x$), respectively; $D_i^{(k)}$, and $D_{ij}^{(k)}$, (i,j = b,c; k=1,2), are the corresponding direct and cross-term interdiffusion coefficients; function *f(x,t)* defines the local volume fraction of the phase 1 in the two-phase mixture, $f(x,t)=V_2/(V_1+V_2)$.

One-dimensional Eqs. (5a) and (5b) are obtained after averaging in the perpendicular to *x* directions as explained in [10]. This averaging procedure is valid for the reaction zone with macroscopic inhomogeneity only in one direction (*x*), i.e. for the layered structure. After this procedure the function *f(x)* becomes smooth and continuous even in the case when the second phase is discontinuous and forms separated precipitates in the first phase matrix.

Concentrations b_1 and c_1 correspond to a single line of the phase diagram (e.g. *ed* in Fig. 3), so, a functional dependence exists between them, j $[b_1(x,t), c_1(x,t)]=0$. Concentrations b_2 and c_2 are not independent either, because at fixed b_1 and c_1 they are completely determined by the equilibrium tie-lines (*dd', ee', ff'*) connecting the points of the equilibrium lines; Fig. 3.

As a result, Eqs. (5) together with corresponding conditions at the two-phase zone boundaries, completely determine the system behaviour, because only two variables are independent: *f(x,t)* and one of the four concentration variables $b_i(x,t)$, $c_i(x,t)$, i=1,2.

III. Qualitative analysis

III.1. Absorption kinetics

Hydrogen absorption kinetics by Zr cladding can be analysed on the basis of the theory developed in [8] and briefly overviewed in subsection II.1. To generalise the theory for description of the low temperature case, one should keep in mind that in accordance with the Zr-H binary phase diagram, Fig. 4 (from [15]) at temperatures below $\approx 550°C$ solubility of hydrogen atoms in the metal matrix drastically falls down. For this reason, hydrogen concentration gradient in the oxide keeps nonzero value for a very long period of time, and hydrogen transported by diffusion through the oxide along this gradient is continuously absorbed (after relatively quick saturation of the metal matrix) in the form of hydride precipitates.

From the flux match at the gas/oxide interface, one can estimate (compare with [8]):

$$p_{H2}(s) \propto J_O^{(ox)}/k \propto \delta(t)^{-1},$$

where *k* is the mass transfer coefficient in the gas phase.

In accordance with Eq. (1):

$$C_{H+}(s) \propto p_{H2}(s)^{1/4} \propto \delta(t)^{-1/4}, \tag{6}$$

thus, substituting this relationship into Eq.(4b) one gets:

$$J_H^{(ox)} = D_H^{(ox)} \Delta C_{H+} / \delta(t) \propto \delta(t)^{-5/4} .$$

Since this flux determines an amount M_H of absorbed hydrogen in the cladding :

$$\partial M_H / \partial t \propto J_H^{(ox)} \propto \delta(t)^{-5/4},$$

finally one can get:

$$M_H \propto \int \delta(t)^{-5/4} dt. \tag{7}$$

At high temperatures (T > 900°C) $\delta(t)$ obeys parabolic kinetics $\propto t^{1/2}$, however, at lower temperatures time dependence $\delta(t) \propto t^n$ is more complicated. For Zr-Nb alloys $n = 0.26$ to 0.65 at T = 400°C [16], and for Zircaloy $n \approx 1/3$ [17] during the initial, pre-transition stage of oxidation. Correspondingly,

$$M_H \propto t^{1-5n/4} \propto t^{9/16} - t^{3/8}. \tag{8}$$

Within the accuracy limits of the hydrogen uptake measurements the difference between the calculated time dependencies from $t^{1/2}$ is insignificant and, therefore, can be sufficiently well described by the parabolic time law. In the post-transition stage hydrogen permeation through the porous oxide layer significantly increases and the fraction of absorbed hydrogen is often close to 100% [4].

III.2. Precipitation and growth of hydrides

For the analysis of the system of Eqs. (5) they can be simplified neglecting H and O fluxes in hydrides in comparison with corresponding fluxes in the metal α-Zr matrix. This is connected with small values of diffuison coefficients in the δ-hydride phase: $D_O^{(\delta)}, D_H^{(\delta)} << D_O^{(\alpha)}$ [18]. The equations can be further simplified owing to an extremely small ratio of the oxygen and hydrogen diffusion coefficients in the α-Zr phase: $D_O^{(\alpha)}/D_H^{(\alpha)} << 1$, which attains several orders of magnitude at T ≈ 400°C [19]. Compensation of such a large value of the hydrogen diffusion coefficient occurs owing to a small value of the hydrogen (solid solution) concentration gradient in the metal phase, $\nabla b_1 \to 0$. However, $b_1(x)$ is not independent function in the two-phase region and is connected with the oxygen concentration distribution in the α-phase $c_1(x)$ by the equation of the equilibrium line *ed* in the phase diagram, Fig. 3: $\nabla b_1 = (\partial b_1/\partial c_1)|_{eq.line} \nabla c_1$, and thus $(\partial b_1/\partial c_1)|_{eq.line} \to 0$. This means that a trajectory of the system in the two-phase region of the equilibrium phase diagram should be restricted by an area corresponding to the condition $(\partial b_1/\partial c_1) \to 0$ along the equilibrium line *de*.

Linearisation of this part of the equilibrium line $b_1 \approx b_1^* + \alpha c_1$ (where $\alpha << 1$) allows representation of hydrogen flux in the α-Zr phase (inside the two-phase region) in the form:

$$J_H = D_H^{(\alpha)}(\partial b_1/\partial c_1)\nabla c_1 + D_{HO}^{(\alpha)} \nabla c_1 \approx \tilde{D}_H \nabla c_1,$$

where $\tilde{D}_H = \alpha D_H^{(\alpha)} + D_{HO}^{(\alpha)}$ is the hydrogen effective diffusion coefficient in the α-Zr phase.

In the result of the above presented simplifications with account of a small oxygen solubility in hydrides ($c_2 << c_1$), the system of Eqs. (5) takes the form:

$$\partial/\partial t[c_1(1 - f)] = D_O \partial/\partial x[(1 - f)\partial c_1/\partial x], \tag{9a}$$

$$\partial/\partial t[b_1(1 - f) + b_2 f] = \tilde{D}_H \partial/\partial x[(1 - f)\partial c_1/\partial x]. \tag{9b}$$

For the analysis of Eqs. (9) it is convenient to introduce a similarity variable $h = (x-x_0)/t^{1/2}$; then the system takes the form ([9]):

$$-(h/2)\partial/\partial h[c_1(h)(1 - f(h))] = D_O[-f'c_1' + (1 - f) c_1''], \tag{10a}$$

$$-(h/2)\partial/\partial h[b_2(h)f(h) + b_1(h)(1 - f(h))] = \tilde{D}_H[-f'b_1' + (1 - f) b_1''], \tag{10b}$$

where $F' \equiv \partial F / \partial h$.

In the considered low temperature case when the oxide layer growth does not obey a parabolic time law, application of the similarity variable transformation becomes not so valuable as it was in the case of the standard parabolic kinetics (e.g. [10]), and the solution of the problem should be searched in a more general formalism of the partial derivative equations, Eqs. (9). Naturally, this makes mathematical analysis of the problem more complicated. However, an exact numerical solution of the problem is beyond the framework of the current paper (lacking necessary detailed experimental data, see below). For a simplified analysis of the problem the deviation of the oxidation kinetics from the parabolic law can be neglected, and application of Eqs. (10) becomes more grounded and elucidating.

It should be additionally noted that such a transformation (to the similarity variable) is completely justified only in the case of a semi-infinite system, or a system with a sufficiently large thickness d (providing large characteristic diffusion times $\sim d^2/D$ in comparison with the observation time τ, i.e. $d^2/D \gg \tau$). In these cases the concentration distributions in various phases is determined by a time-invariable trajectory in the equilibrium phase diagram, which allows a simple solution of the problem (compare with [10]).

In the considered case the required condition $d^2/D \gg \tau$ is valid only for oxygen, however, is not valid for hydrogen owing to its high diffusivity in the α-Zr phase. In particular, this leads to the time variation of the system trajectory through the two-phase region of the phase diagram (see below). Nevertheless, this difficulty can be overcome by application of the quasi-stationary approximation, which becomes valid owing to a relatively slow variation of the trajectory (in comparison with the rapid hydrogen diffusion). In this approximation a solution of Eqs. (10) is searched assuming fixed (but unknown) position of the trajectory; after the solution is found the position of the trajectory is determined self-consistently from the mass conservation law.

The superposition of the Eqs. (10) yields:

$$(D_O / \tilde{D}_H) \partial / \partial h [b_2 f + b_1 (1 - f)] = \partial / \partial h [c_1 (1 - f)]. \tag{11}$$

Since the hydrogen concentration gradient in the α-Zr phase is small, $b_1(h)$ can be considered as a constant value, i.e. $\partial b_1 / \partial h \approx 0$. Thus, integration of Eq. (11) yields:

$$(D_O / \tilde{D}_H)(b_2 - b_1) f - c_1 (1 - f) = \text{const}. \tag{12}$$

The obtained equation describes inhomogeneous distribution of $f(x,t)$ along the oxygen concentration profile in the α-Zr phase. Outside the oxygen concentration front $f(x,t)$ becomes spatially homogeneous (due to the rapid hydrogen diffusion in the metal phase) and slowly growing with time (due to the continuous hydrogen supply), i.e. $f(x,t) = f_0(t)$.

Namely this value $f_0(t)$ determines the ratio of the tie-line lengths $Ee':Ee$ (see Fig. 3) and, therefore, the position of the two-phase trajectory DE in the equilibrium phase diagram. At fixed value $f_0(t)$ the constant in the r.h.s. of Eq. (12) is equal to $(D_O / \tilde{D}_H) \Delta b f_0$, where $\Delta b = b_2 - b_1$ (since $f \to f_0$, when $c_1 \to 0$). Correspondingly, the solution of Eq. (12) takes the form:

$$f = [(D_O / \tilde{D}_H) \Delta b f_0 + c_1] / [(D_O / \tilde{D}_H) \Delta b + c_1]. \tag{13}$$

By substitution of Eq. (13) in Eq. (10a) one can calculate $c_1(h)$ and $f(h)$ (see Fig. 5). In its turn this allows calculation of the hydrogen content variation in the cladding, which coincides with the hydrogen flux $J_H^{(ox)}$ from oxide (see Eq. (4b)) and/or from the gas phase:

$$J_H^{(ox)} \approx b_2 \partial / \partial t (\int f \, dx). \tag{14}$$

Finally, the self-consistent solution of Eqs. (4b), (10a), (13) and (14) determines the value $f_0(t)$.

It should be noted that the final solution was found on the base of the equilibrium line linearisation $b_1 \approx b_1^* + \alpha c_1$ in the beginning of calculations. Therefore, a possible variation of the parameter α (which determines the value of the hydrogen effective diffusion coefficient $\tilde{D}_H = \alpha D_H^{(\alpha)} + D_{HO}^{(\alpha)}$) along the system trajectory can additionally change the distribution function $f(x,t)$. In particular, if α is not too small and thus $\tilde{D}_H \gg D_O^{(\alpha)}$, then $f \to 1$, i.e. locally occupation of the matrix by hydrides can be very high (e.g. near the interface with oxide).

In order to perform more detailed numerical calculations one needs additional data on the system parameters and behaviour (interface concentrations in various phases, oxygen concentration and hydride distribution profiles, etc.). These data can be obtained from the detailed metallography examinations of the samples (compare with [10]). Nevertheless, the obtained analytical solution, Eq. (13) correctly describes the main qualitative features of the observations. Indeed, in accordance with this equation two regions of hydride distribution exist in the metal matrix. In the vicinity of the oxide/metal interface the oxygen concentration profile exists which disappears in the bulk of the metal phase. The hydride distribution function (i.e. their specific volume in the matrix) is tightly connected with the oxygen profile and steeply decreases in the bulk. It attains a certain value f_0 at the oxygen concentration front and becomes spatially homogeneous beyond this front. Along with the oxygen front penetration in the metal cladding of the high burnup fuel rods, the depth of the non-homogeneous hydride distribution region increases and simultaneously increases the volume of hydrides in the outer region. The largest amount of hydrides is sustained near the oxide/metal interface, leading to the brittle mechanical behaviour of the cladding and PCMI failure of the high burnup fuel rods.

IV. Conclusions

In the present paper modelling of the complicated behaviour of hydrogen in the oxidising Zry cladding observed in the high burnup fuel tests, is attempted. The previously developed model for hydrogen absorption by Zr alloys during oxidation in steam and mass transfer through the growing oxide scale at high temperatures, is further applied to the low temperature case and predicts close to parabolic hydrogen absorption kinetics in the pre-transition stage of corrosion. The consideration of hydrogen and oxygen diffusion transport in the metal Zry matrix with growing hydrides is based on the other previous approach to the modelling of the multicomponent diffusion in the two-phase zone. This allows self-consistent calculation of the spatial profiles of the oxygen concentration and hydride distribution in the metal cladding, and results in the natural explanation of the observed steep spatial gradient in the hydride distribution. In accordance with the current knowledge, this hydriding effect leads to the brittle mechanical behaviour of the cladding and PCMI failure of the high burnup fuel rods.

References:

1. J. Papin, M. Balourdet, F. Lemoine, J.M. Frizonnet, F. Schmitz, French studies on high-burnup fuel transient behaviour under RIA conditions, in: Reactivity-Initiated Accidents (special issue) Nuclear Safety 37(4) (1996).

2. T. Fuketa, F. Nagase, K. Ishijima, T. Fujishiro, NSRR/RIA experiments with high-burnup fuels, in: Reactivity-Initiated Accidents (special issue) Nuclear Safety 37(4) (1996).

3. F. Schmitz, J. Papin, J. Nucl. Mater. 270 (1999) 55.

4. B. Cox, Advances in Corrosion Science and Technology, 5(1976)173.

5. Y. Kim, W.-E. Wang, D.R. Olander and S.K. Yagnik, J. Nucl. Mater. 240 (1996) 27.

6. G. Meyer, M. Kobrinsky, J.P. Abriata, J.C. Bolcich, J. Nucl. Mater. 229 (1996) 48.

7. J. Freska, G. Konczos, L. Maroti, L. Matus, Oxidation and Hydriding of Zr1%Nb Alloys by Steam, Report KFKI-1995-17/G, 1995.

8. M.S. Veshchunov, A.V. Berdyshev, J. Nucl. Mater. 255 (1998) 250.

9. M.S. Veshchunov, P. Hofmann, J. Nucl. Mater. 210 (1994) 11.

10. M.S. Veshchunov, P. Hofmann, J. Nucl. Mater., 236 (1995) 72.

11. C. Wagner, Ber. Bunsen-Ges. Phys. Chem. 72 (1968) 778.

12. K. Park, D.R. Olander, J. Am. Ceram. Soc. 74 (1991) 72.

13. T.F. Bowe, H.D. Brody and M.C. Flemings, Trans. AIME 227 (1963) 374.

14. M.C. Flemings, Solidification Processing, McGraw-Hill, New York, 1974.

15. O. Kubashchewski-von Goldbeck, in: Physico-Chemical Propreties of the Compounds and Alloys, Part II: Phase Diagrams, IAEA Special Issue 6 (1976) 88-90.

16. K.-N. Choo, S.-I. Pyun, Y.-S. Kim, J. Nucl. Mater., 226 (1995) 9.

17. A.J.G. Maroto, R. Bordoni, M. Villegas, A.M. Olmedo, M.A. Blesa, A. Iglesias, P. Koenig, J. Nucl. Mater. 229 (1996) 79.

18. A. Sawatzky and E. Vogt, Trans. Metall. Soc. AIME 227 (1963) 917.

19. A. Sawatzky, J. Nucl. Mater. 2 (1960) 62.
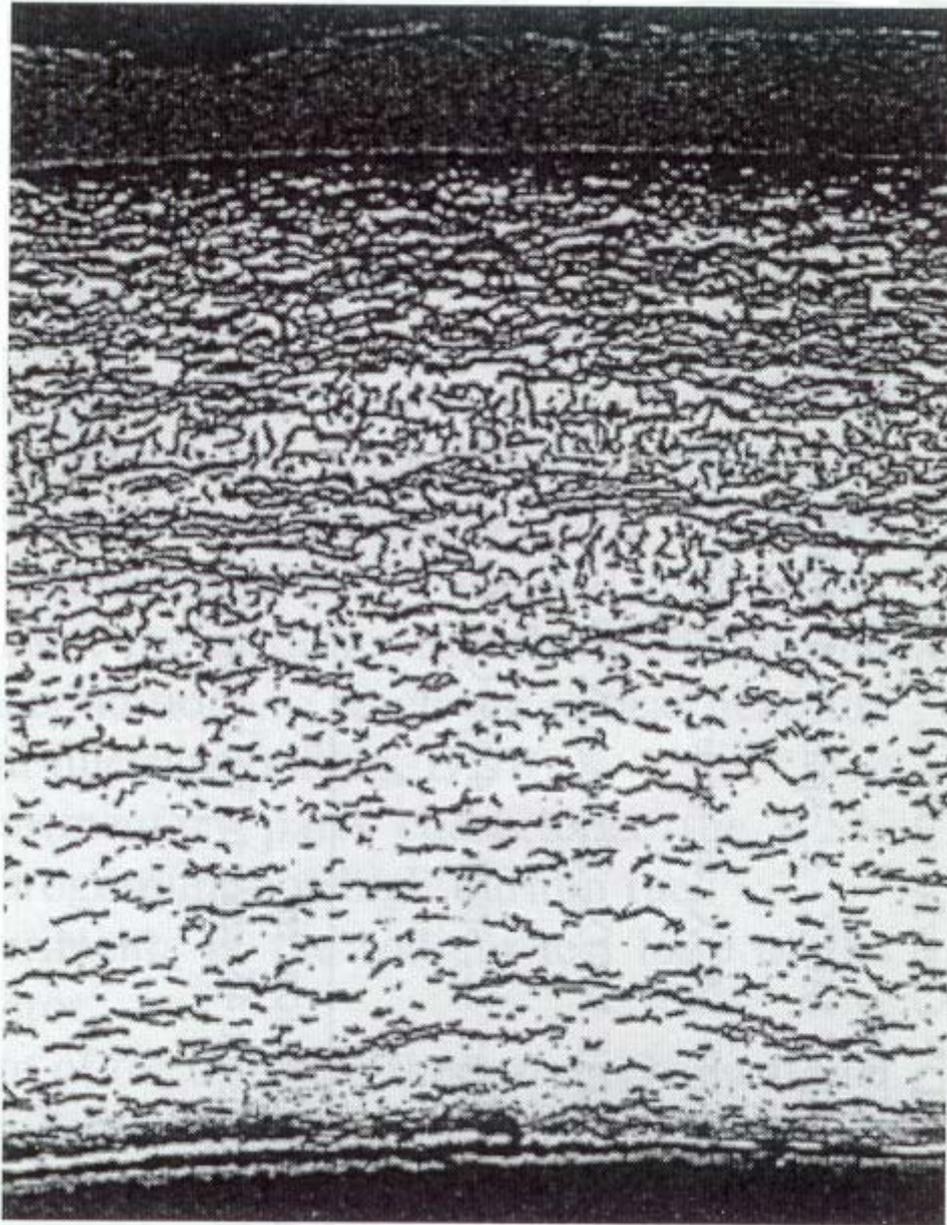
Fig. 1: Metallographic cut of the rod cladding after CABRI test [1,3] with hydride plates revealed by etching.

Fig. 2: Metallographic cut of the rod cladding after HBO test [2] with brittle cracks in the hydrided zone.
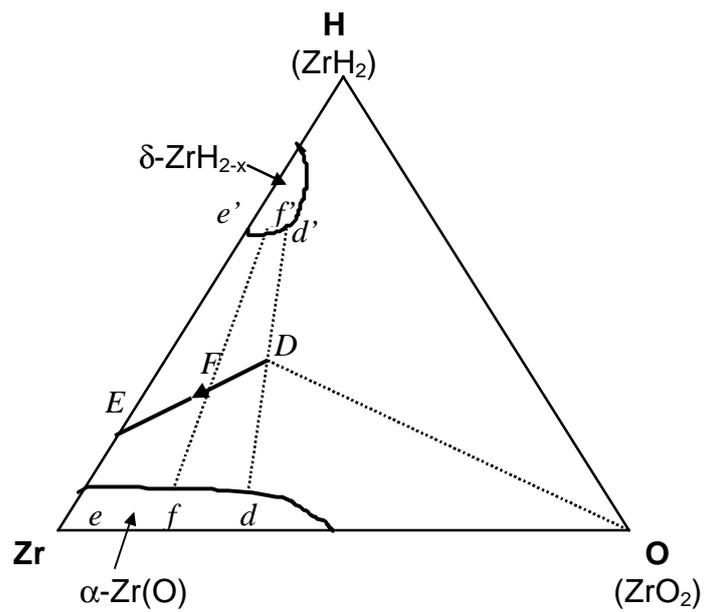
Fig. 3:   Schematic ternary Zr-O-H phase diagram with the diffusion path *DE*

13
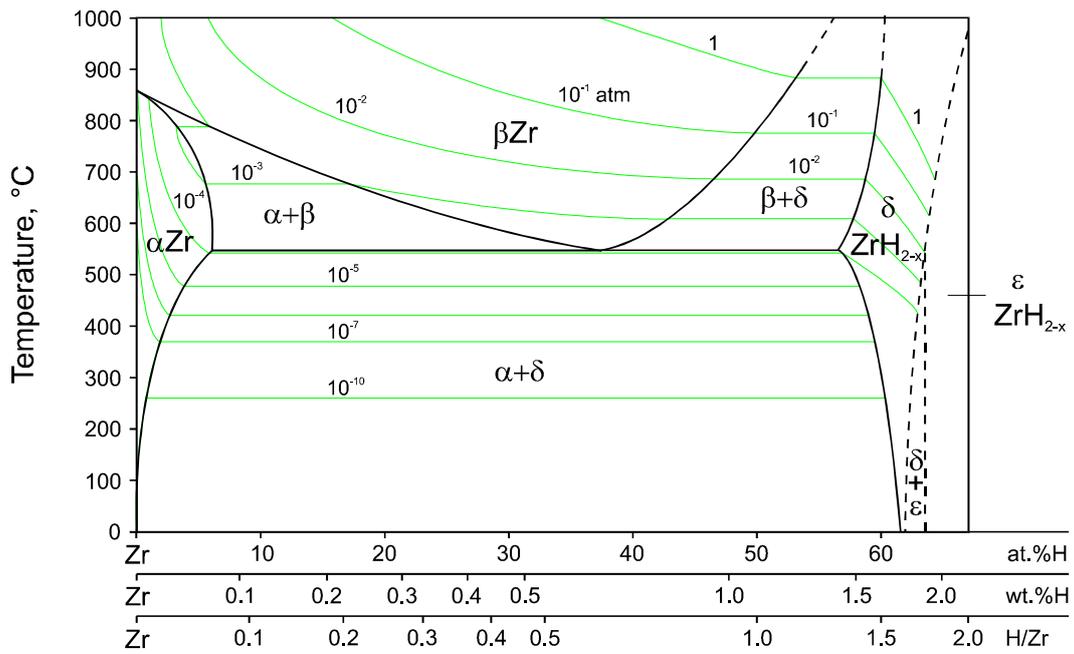
Fig. 4: Binary Zirconium-Hydrogen phase diagram and equilibrium hydrogen pressures (from [15]).
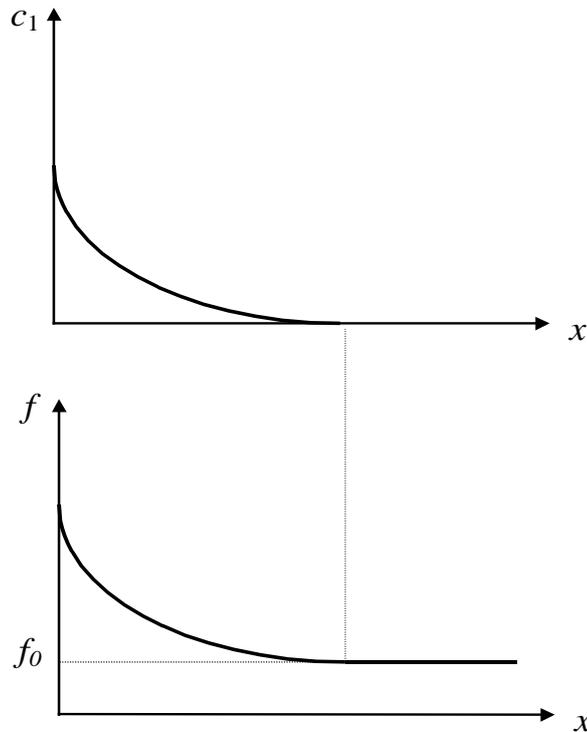
Fig. 5: Schematic presentation of spatial profiles of the oxygen concentration $c_1(x)$ and hydride distribution function $f(x)$ in the metal cladding.